

RI 8984

Bureau of Mines Report of Investigations/1985

Plasma-Sprayed Iron-Base Wear-Resistant Coatings Containing Titanium Diboride

By J. F. McIlwain and L. A. Neumeier



UNITED STATES DEPARTMENT OF THE INTERIOR



Report of Investigations 8984

Plasma-Sprayed Iron-Base Wear-Resistant Coatings Containing Titanium Diboride

By J. F. McIlwain and L. A. Neumeier



UNITED STATES DEPARTMENT OF THE INTERIOR
Donald Paul Hodel, Secretary

BUREAU OF MINES
Robert C. Horton, Director

Library of Congress Cataloging in Publication Data:

McIlwain, J. F

Plasma-sprayed iron-base wear-resistant coatings containing titanium diboride.

(Report of investigations / United States Department of the Interior, Bureau of Mines ; 8984)

Bibliography: p. 18.

Supt. of Docs. no.: I 28.23:8984.

1. Hard-facing. 2. Hard-facing alloys. 3. Titanium diboride. I. Neumeier, L. A. II. Title. III. Series: Report of investigations (United States. Bureau of Mines) ; 8984.

TN23.U43 [TS227.3] 622s [671.7] 85-600122

CONTENTS

	<u>Page</u>
Abstract.....	1
Introduction.....	2
Acknowledgment.....	3
Alloy system characterization.....	3
Experimental procedure.....	5
Powder preparation.....	5
Plasma spraying.....	8
Physical and mechanical testing.....	10
Results.....	10
Discussion.....	16
Summary and conclusions.....	17
References.....	18

ILLUSTRATIONS

1. Differential thermal analysis.....	4
2. Derived phase boundaries in pseudobinary section.....	5
3. Microstructures of cast alloys H26 and H28.....	6
4. Effect of TiB_2 (equivalent) on the impact energy and ferrite number.....	6
5. Micrographs showing progression of homogenization and attrition.....	7
6. Effect of milling time on oxygen content of mechanically alloyed powders..	8
7. Water-cooled plasma torch and specimen holder.....	9
8. Abrasive-wear test apparatus.....	11
9. Adhesive-wear test apparatus.....	12
10. Diffraction-interference contrast micrographs.....	13
11. Porosity of plasma-sprayed coatings.....	14
12. Hardness of cast and plasma-sprayed alloys.....	14
13. Linear relationship between abrasive weight loss and cycles.....	15
14. Abrasive-wear rates of plasma-sprayed coatings.....	15
15. Relation between decrease in oxygen content of plasma-sprayed powders.....	17

TABLES

1. Critical metal content of alloys.....	2
2. Composition of cast iron-base superalloy heats.....	4
3. Chemical analysis of cast superalloy heats.....	4
4. Nominal purity and analyzed oxygen content of starting powders.....	6
5. Chemical analysis of mechanically alloyed powders.....	8
6. Bond strengths of plasma-sprayed coatings.....	14
7. Adhesive wear data for plasma-sprayed coatings.....	15

UNIT OF MEASURE ABBREVIATIONS USED IN THIS REPORT

A	ampere	L	liter
°	degree	MPa	megapascal
°C	degree Celsius	μm	micrometer
DPH	diamond-pyramid hardness	mg	milligram
ft•lbf	foot pound (force)	mm	millimeter
g	gram	min	minute
h	hour	nm	nanometer
J	joule	rpm	revolution per minute
kg	kilogram	vol pct	volume percent
kW	kilowatt	wt pct	weight percent

PLASMA-SPRAYED IRON-BASE WEAR-RESISTANT COATINGS CONTAINING TITANIUM DIBORIDE

By J. F. McIlwain¹ and L. A. Neumeier¹

ABSTRACT

Cobalt-base hardfacing alloys used for wear resistance consist almost entirely of metals largely imported into the United States. As part of an overall research program to help alleviate this foreign dependency, the Bureau of Mines has been investigating an iron-base alloy system as a potential replacement for cobalt-base alloys for some uses. To ascertain the melting ranges, thermal analyses were made of cast heats of alloys containing, in weight percent, 59-61 Fe, 16-19 Cr, 8-9 Ni, 1 Mn, 1 W, 1 Mo, 0.5 Cb, 0.6 Si, 0.3 C, and 0-12 stoichiometric TiB₂. Powder alloys within this range of composition, prepared by mechanical alloying, were sized and applied to mild steel test coupons by nontransferred-arc plasma spraying. The resulting thin coatings were >95 pct dense, with bond strengths of 35 MPa and hardness of 400 to 840 DPH. Abrasive and adhesive wear test data were compared to those of a plasma-sprayed cobalt-base alloy. A range of boride contents resulting in most promising properties was determined for further research.

¹Supervisory metallurgist.

Rolla Research Center, Bureau of Mines, Rolla, MO.

INTRODUCTION

Wear is a destructive phenomenon rivaling corrosion in terms of cost to the economy. In the United States, the annual cost due to wear has been estimated at \$60 billion (1).²

One means of combatting wear is the application of wear-resistant coatings or overlays to either partially worn parts or original equipment. Alloys tailored to specific wear situations may be used as hard coatings in conjunction with tougher, more economical structural materials. Most of these hard, wear-resistant alloys contain significant fractions of strategic and critical metals such as Cr, Co, Ni, and Mn. In particular, the cobalt-base Stellite³ series of alloys consist of more than 90 pct Cr, Co, and W. They are used as weld-deposited or thermally sprayed coatings.

The cobalt-base hardfacing alloys have found numerous applications in minerals-related and other industries. Such uses include exhaust valves, steam engine valve trim, and pump shafts (2), pumps and fittings in chemical processing industries (3), rotary valves in wood pulp digesters (4), arbors and machine knives in the brick and clay industry, cement conveyor pipes, ash plows, hot-work dies, heat-treating lead pots, ingot tongs and bits, hot-shear blades, skip-hoist cable sheaves in mining, and hot-oil pump sleeves (5). Cobalt-base coatings are also used to resist the hot abrasion of alumina-silica catalysts in fluid-catalytic cracking unit feed nozzles (6).

In reaction to the cobalt shortage of the late 1970's, a number of prospective replacement alloys emerged. Most of these are nickel-based. Table 1 lists the compositions of a number of these, as well as those of some of the traditional

cobalt-base alloys. Haynes alloy N-6 reportedly exhibits hot hardness superior to that of Stellite 6 and Haynes 716, both of which behave similarly (8). Adhesive wear resistance of both of these replacement alloys is an order of magnitude better than that of Stellite 6 and slightly better than that of the harder Stellite 1. Both of these nickel-bearing alloys abrade at about the same rate as Stellite 6 but have only about 60 pct of its impact strength. The corrosion properties of Haynes N-6 are similar to those of Stellite 6. Haynes 711, compared to Stellite 6, has 10 to 30 pct lower hot hardness, about one-half of the abrasive wear resistance, and superior adhesive wear resistance. The corrosion resistance of Haynes 711 and 716, due to their higher iron contents, is equal to or worse than that of the high-cobalt Stellite alloys they are intended to replace. Alloys SN-81A and SN-86A approximate the composition of Stellite alloys 1 and 6, respectively (9), with about 20 pct Ni substituting for a corresponding amount of cobalt. Although fewer data are available for these alloys, compared with data regarding Stellite alloys 1 and 6 (table 1), their room-temperature hardness values are known to be higher.

TABLE 1. - Critical metal content of cobalt-base and substitute wear-resistant alloys

Alloy	Critical metal content, wt pct				Reference
	Co	Cr	Ni	W	
Stellite 1...	¹ 55	30	0	12	7
Stellite 6...	¹ 67	28	0	4	7
Stellite 31...	¹ 56	26	10	7	7
Haynes N-6...	0	26	¹ 62	2	8
Haynes 711...	12	27	¹ 22	3	8
Haynes 716...	12	26	23	3.5	8
SN-81A.....	28	21	25	14	9
SN-86A.....	33	29	20	6	9
VMS 585 ²	0	24	11	0	10
XN-930C.....	0	30	¹ 54	0	11

¹Approximate value; listed as "balance" in references.

²57 pct Fe.

²Underlined numbers in parentheses refer to items in the list of references at the end of this report.

³Trade names of Wear Technology Division, Cabot Corp., Kokomo, IN. Reference to specific products does not imply endorsement by the Bureau of Mines.

Abrasive slurry testing indicated 55 pct improved wear resistance for SN-81A and equivalent wear for SN-86A. These alloys display large, blocky carbides. Commercial applications were not indicated.

At about 57 pct Fe, VMS 585 is the "leanest" alloy of the group described in table 1 (10). It was developed especially for plasma-transferred arc-valve facing applications with lead-free fuels, where PbO corrosion of iron would not be a problem. Hot hardness and adhesive wear (crossed-cylinder test with a high-carbon, nickel-base alloy) results nearly duplicated those of Stellite 6. Sulfidation corrosion weight loss for 80 h at 870° C in a mixed salt bath was 39 pct that of the Stellite.

The Ni-Cr-Mo-C alloy XN-930C also employs blocky, hypereutectic carbides for wear resistance (11). It exhibits 7 to 10 times better adhesive wear than Stellite 6 when mated to M6 tool steel. Hot hardness was 10 to 20 pct higher up to 815° C, while abrasive wear was nearly equivalent.

It is seen that although a number of substitute alloys have emerged, for the

most part they remain high in imported or critical metals. Because of this and the wide usage of the cobalt-base alloys, a candidate alloy system, lower in critical metals, was sought by the Bureau of Mines as a potential substitute for the high-cobalt alloys in selected applications. Initial research emphasized investigation of the effectiveness of adding hard borides to improve the wear resistance of a carbide-strengthened, heat-resistant alloy system based on the commercial iron-base superalloy 19-9DL. The system contains no cobalt, less than 20 pct of chromium and less than 10 pct of nickel, and minimal tungsten and manganese. Titanium diboride (TiB_2) is the added hard-particle phase. The experimental alloys were prepared as mechanically alloyed powders for subsequent application by thermal spraying of thin coatings or weld deposition of thicker coatings to steel substrates. Stellite 6 was selected as a standard of comparison. This report describes the results of the research on plasma-sprayed coatings on steel substrates.

ACKNOWLEDGMENT

The authors wish to acknowledge the work of A. J. Mackie at the Albany (Oreg.) Research Center, Bureau of Mines, in performing scanning electron

microscope (SEM) and electron microprobe examinations of cast and plasma-sprayed samples.

ALLOY SYSTEM CHARACTERIZATION

To help characterize the iron-base TiB_2 -bearing alloy system, a series of cast heats was made using heat sizes of 500 to 800 g. Elemental starting materials were charged to an induction furnace crucible operating in a chamber under 1 atm of helium. Carbon and boron, as briquetted powder compacts, were added to the molten charge 10 min prior to pouring the melts into iron molds.

Table 2 lists the nominal compositions of the heats (H). Chemical analyses were performed by induction furnace combustion for carbon, ion exchange and volumetric titration or inductively coupled

plasma (ICP) for boron, and ICP for titanium. Other elements were analyzed by ICP or by conventional wet analyses. The analyses, given in table 3, indicate some loss of titanium during melting or possibly incomplete detection. Boron losses appeared to be about 10 pct.

Each of the cast heats was subjected to differential thermal analysis (DTA) using a Netzsch thermal analyzer. Samples of typically 200 mg were heated at 10° C/min under flowing helium to 1,550° C. The differential heating curves, corrected for background drift and normalized to unit sample mass, are shown in figure 1.

Temperatures corresponding to peaks in the curves were taken to represent phase changes, with the highest peak in each curve representing the liquidus. The resulting points are laid out in figure 2 to form a pseudobinary phase diagram of

TABLE 2. - Composition of cast iron-base superalloy heats containing titanium and boron additions

(Nominal composition,¹ weight percent)

Heat	Cr	Ni	Mn	Mo	W	Cb	Si	C	Ti	B
H16.....	19.0	9.0	1.0	1.0	1.0	0.5	0.4	0.30	0	0
H24.....	19.0	9.0	1.0	1.0	1.0	.5	.4	.30	.03	.015
H18.....	19.0	9.0	1.0	1.0	1.0	.5	.4	.30	.17	.075
H19.....	18.8	8.9	1.0	1.0	1.0	.6	.4	.30	.83	.375
H25.....	18.4	8.7	1.0	1.0	1.0	.5	.4	.29	2.00	.910
H26.....	17.9	8.5	.9	.9	.9	.5	.4	.28	4.10	1.86
H27.....	17.3	8.2	.9	.9	.9	.4	.4	.27	6.30	2.85
H28.....	16.6	7.8	.9	.9	.9	.4	.4	.26	8.90	4.00

¹Balance Fe.

TABLE 3. - Chemical analysis of cast superalloy heats containing titanium and boron additions

(Analyzed composition, weight percent)

Heat	Ti	B	C	Heat	Ti	B	C
H16.....	<0.01	0.03	0.30	H25.....	1.5	0.89	0.28
H24.....	.02	.04	.33	H26.....	4.3	1.40	.29
H18.....	.04	.09	.31	H27.....	5.0	2.60	.30
H19.....	.73	.37	.31	H28.....	6.5	3.60	.27

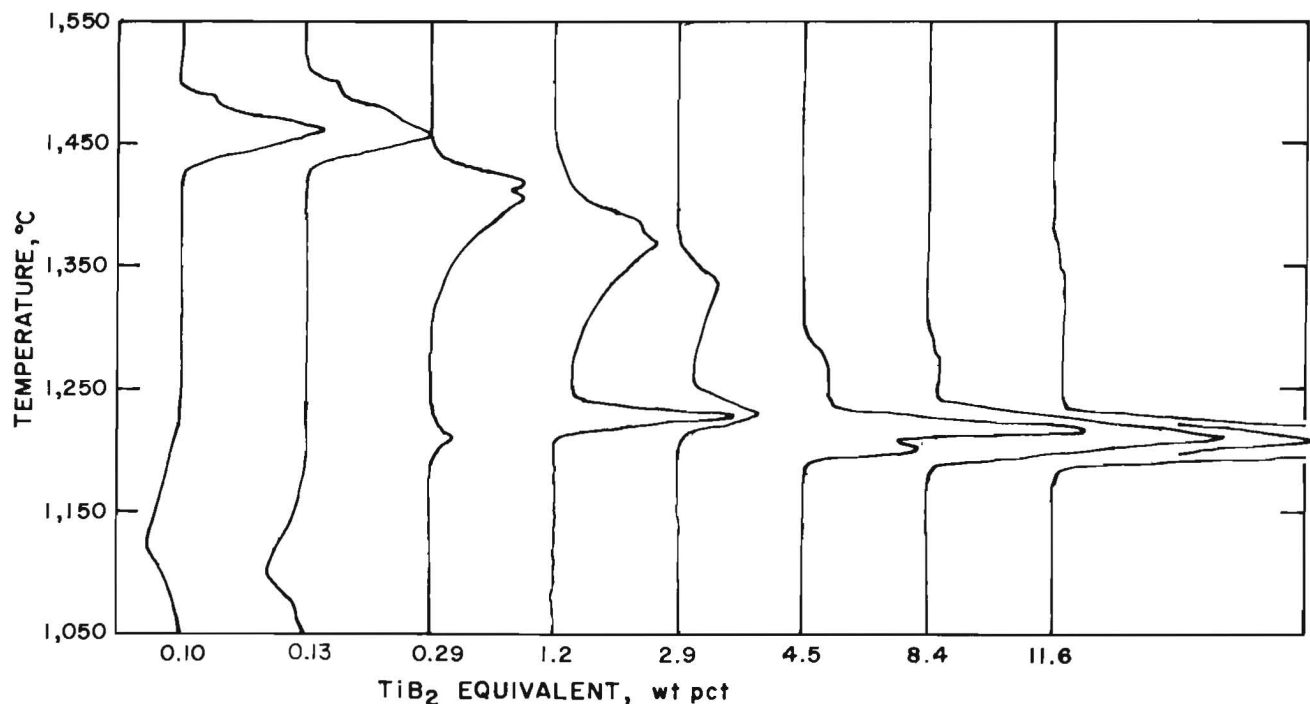


FIGURE 1. - Differential thermal analysis curves for cast alloys with various TiB_2 equivalents.

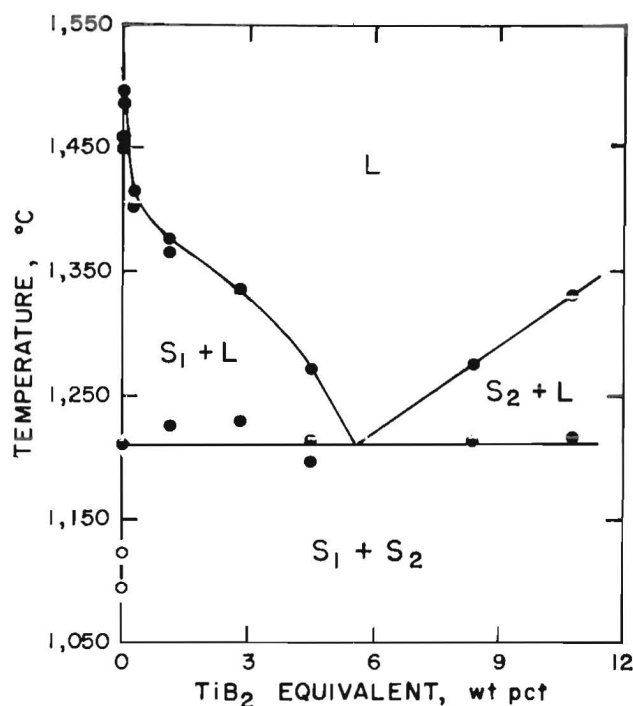


FIGURE 2. - Derived phase boundaries in pseudo-binary section as a function of TiB_2 equivalent. S_1 , S_2 , and L indicate solid and liquid phases.

the matrix alloy versus titanium diboride, calculated from the analyzed values of boron. In these and ensuing references to the cast alloys, the titanium and boron contents are designated as " TiB_2 equivalent" based on the boron content. This designation is for convenience in describing the results and does not imply the existence of TiB_2 as a discrete phase in each instance. This is not a rigorous treatment of the system. First, in these melted alloys, the titanium and boron may not exist in a substantial amount as a discrete titanium boride (TiB_2) in the presence of the other boride formers such as Cr, W, Cb, and Mo. A second consideration is that the sample material is in the as-cast condition, which is not the equilibrium state. Perhaps reflecting this condition

are the apparently anomalous "double peaks" at 0.13 and 4.50 wt pct boride and the exothermic peaks associated with curves for the two samples with lowest boron content.

Despite the stated complexities, the data do reflect the general behavior of the system. The solidus and liquidus temperatures at 0 pct TiB_2 are consistent with (12) for 18 pct Cr-8 pct Ni steel with 0.3 pct C and with the melting range of 19-9DL (13). The overall eutectic structure is characteristic of binary metal-boron systems such as Fe-B, Cr-B, Ni-B, and the pseudobinary Fe- TiB_2 (14), although the sharp decrease in liquidus with small additions of boron is unique to the present system. As with the binary system, virtually no solid solubility of boron in the iron-base solid solution is indicated.

The microstructure of the hypoeutectic compositions is dendritic austenite (fig. 3A), while the hypereutectic composition shows the addition of blocky and acicular phases (fig. 3B). These second phases are accompanied by an increased magnetic fraction, as determined by Magnegage measurements and included in the plots in figure 4. The Charpy unnotched impact energy data, included in figure 4, serve to show the rapid embrittlement of the alloys up to about the eutectic composition, followed by fixed low values. Samples from heats H26 and H28 were evaluated with a scanning electron microscope (SEM) and an electron microprobe. The interdendritic phase was high in Ti, Cr, and W, probably as carbides, in both alloys. The proeutectic phases were tentatively identified as acicular delta ferrite containing about 45 wt pct Fe and 51 wt pct Cr, plus blocky TiB_2 . Nearly all of the ferrite needles were associated with a blocky boride precipitate.

EXPERIMENTAL PROCEDURE

POWDER PREPARATION

Powders for plasma-spray coating were prepared by the mechanical alloying of elemental and binary powders. This technique can produce quasi-alloy powder

from simple components by repeated cold-welding and fracturing of the powder particles (15). Alloying is done by dry milling in a 9.5-L-capacity, high-speed, stirred ball mill known as an attritor. Starting powders were minus 80 mesh or

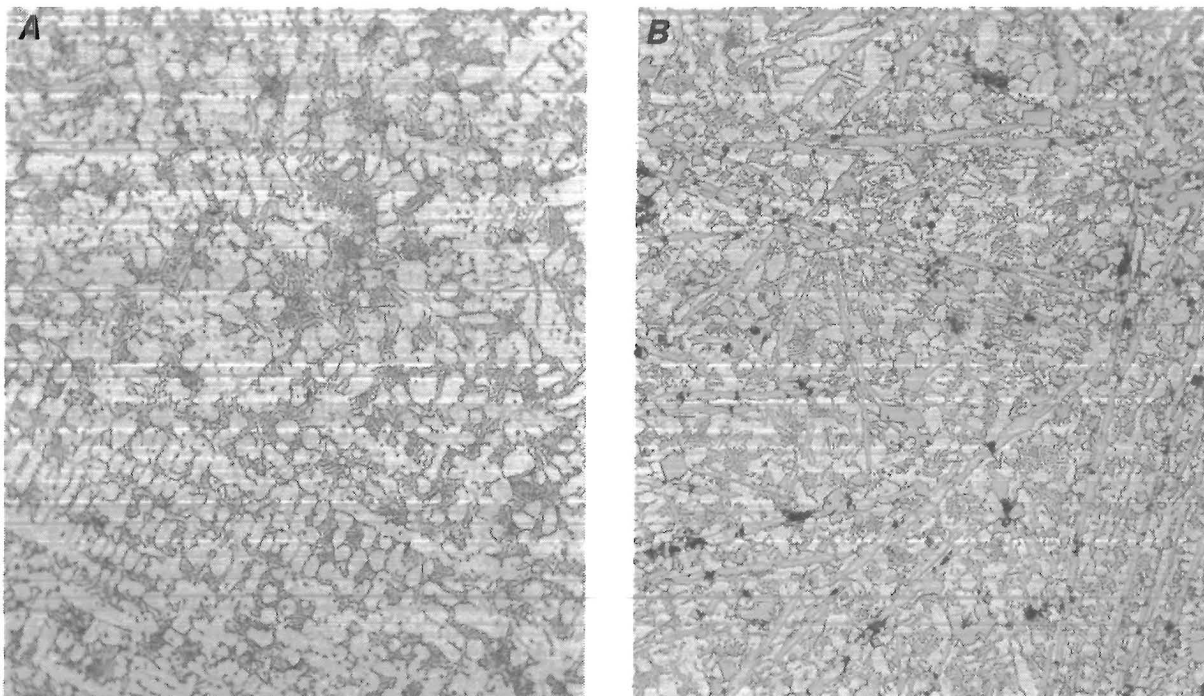


FIGURE 3. - Microstructures of cast alloys (X 250). A, H26; B, H28. Heat H26, with 4.5 wt pct TiB_2 equivalent, shows interdendritic carbides with an austenitic matrix. At 11.6 wt pct TiB_2 equivalent, heat H28 shows proeutectic TiB_2 (blocky phase) and ferrite (acicular phase). Glyceregia etch.

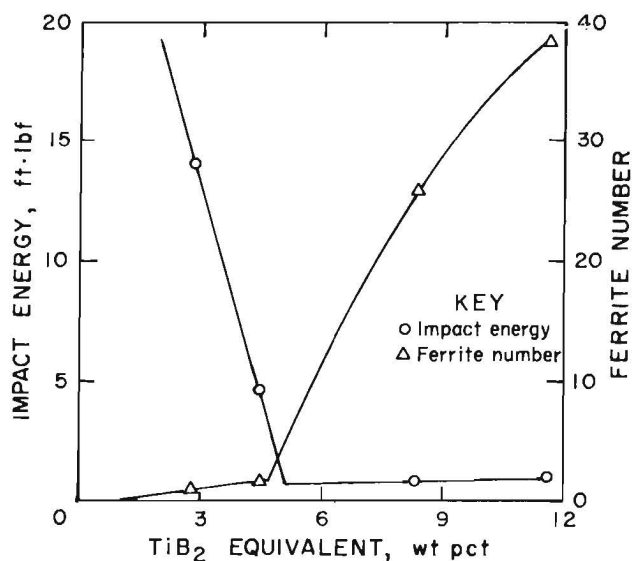


FIGURE 4. - Effect of TiB_2 (equivalent) on the impact energy and ferrite number of cast alloy heats (1 ft·lbf = 1.36J).

finer. Table 4 lists the nominal purity specified by the supplier, and analyzed oxygen content, determined by inert gas fusion, of the starting powders. Carbon was added as graphite powder. Compositions nominally equivalent to those of

TABLE 4. - Nominal purity¹ and analyzed oxygen content of starting powders

Powder	Nominal purity, wt pct	Oxygen, wt pct
Fe.....	99.3	0.17
Cr.....	99.2	.39
Ni.....	99.2	.14
Mn.....	99.4	.55
Mo.....	99.9	.27
W.....	99.9	.36
Cb.....	99.5	.49
Si.....	98.0	.46
TiB ₂	99.0	.36

¹As specified by supplier.

cast heats H16 and H25 through H28 were prepared.

Mixtures totaling 1 kg were blended in a double-cone blender for 30 min and were then charged to the attritor chamber. Hardened-steel balls of 9.52 mm diameter served as the grinding medium at a ball-to-powder ratio of 18. Prior to milling, the chamber was flushed with pure argon for 30 min, sufficient to reduce the oxygen level to <0.1 pct.

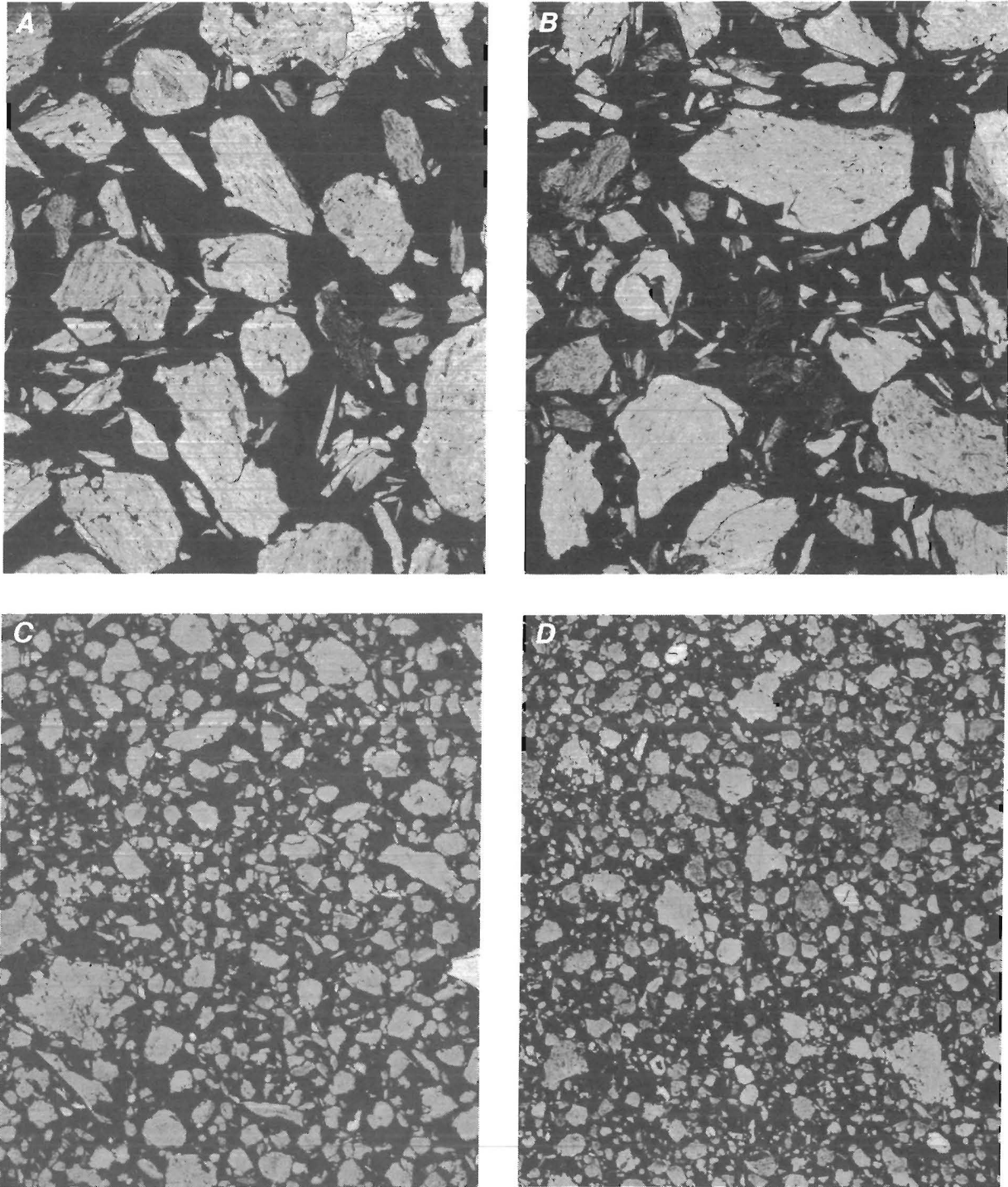


FIGURE 5. - Micrographs showing the progression of homogenization and attrition during mechanical alloying of metal powders containing 9.2 wt pct TiB_2 (X 100). *A*, 24 h milling time; *B*, 48 h; *C*, 74 h; and *D*, 97 h. Glyceria etch.

The powders were dry milled at 300 rpm for 65 to 100+ h. Particle homogenization ("alloying") and uniform boride dispersion were accomplished by 70 h; the additional milling was necessary to increase the yield of minus 325-mesh powder. Figure 5 illustrates the progressive attrition and homogenization of a batch of powder containing nominally 9.2 wt pct TiB_2 . Two charges of nominally boride-free powder produced such small quantities of fine powder (<5 pct) that they were subsequently milled for 8 h under ethanol. This attrition grinding produced 74 pct of minus 325-mesh powder, a typical value for the other compositions under dry milling conditions. All powders intended for plasma spraying were screened to minus 325 mesh. This fraction was further sized in an air elutriator to remove the minus 10- μm fines, thus yielding a powder size range of 44 to 10 μm .

Despite the protective atmosphere inside the chamber, some air leakage occurred and the powders picked up oxygen. The repeated fracturing of the particles exposed atomically clean surfaces which readily oxidized. Upon rewelding, the oxide was incorporated into the particles. The linear adsorption rate with milling time is illustrated in figure 6. The starting oxygen contents were calculated from the starting powder values. Oxygen levels of the milled powders appear in table 5, along with the analyzed boron and nitrogen contents. Nitrogen pickup was substantially less than oxygen pickup and was relatively constant.

PLASMA SPRAYING

Sample coatings were prepared by non-transferred-arc plasma-spraying of the powders onto mild steel substrates. The sizes and shapes of the various test pieces used are described in the following section. The plasma unit was a 40-kW spray system operating in the high-voltage mode. Premixed Ar-10 pct H_2 served as the arc gas; the powder feed gas was argon. A stream of argon swept the substrate surface ahead of the beam to reduce oxidation. For spraying, test pieces were mounted in a standard

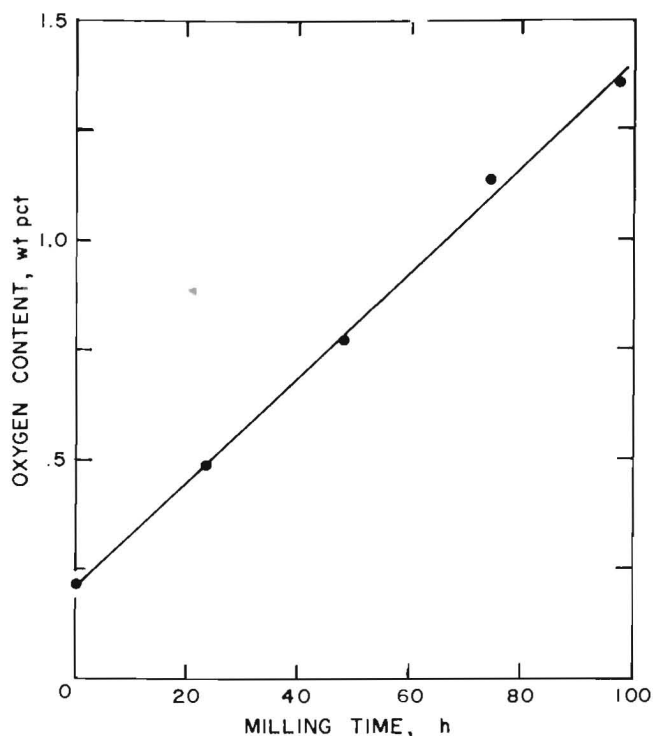


FIGURE 6. - Effect of milling time on oxygen content of mechanically alloyed powders.

TABLE 5. - Chemical analysis of mechanically alloyed (MA) powders

(Analyzed contents, weight percent)

Batch	B	O	N
MA1.....	0.03	0.58	0.11
MA2.....	.85	1.80	.23
MA3.....	1.65	1.23	.11
MA4.....	2.3	.63	.11
MA5.....	2.9	.73	.17

machinist's lathe at a distance of 50 to 75 mm from the plasma gun (fig. 7). Prior to spraying, the coupons were deoiled, sandblast cleaned with alumina, then coarsened to 5- μm arithmetic-average (AA) surface roughness using clean SiC grit. Powder feeds of 10 to 15 g/min with arc currents of 250 to 380 A were used. Specific conditions were adjusted to optimize coating density and bonding. For comparison, Stellite 6 powder of minus 325-mesh particle size, obtained from a commercial source, was plasma-sprayed under similar conditions.

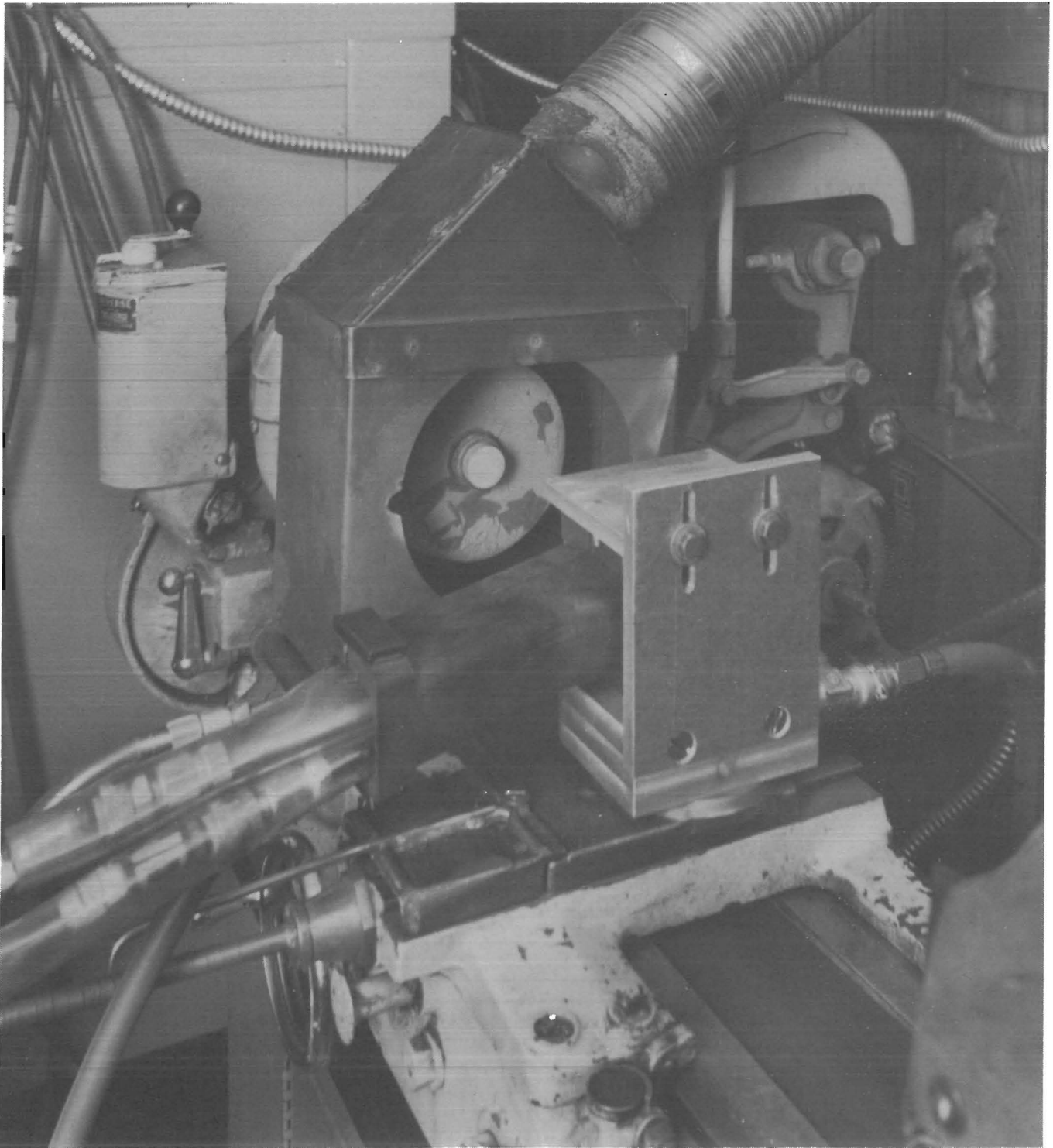


FIGURE 7. - Water-cooled plasma torch and specimen holder. Torch is fixtured to provide horizontal motion at constant distance to specimen. A coated 25-mm-diam specimen is mounted in a lathe chuck inside a ventilation hood.

PHYSICAL AND MECHANICAL TESTING

A number of physical examinations and mechanical property tests were performed on the sprayed coatings. The sizes and configurations of the mild steel test coupons (substrates) used are described in succeeding paragraphs. The tests evaluated some physical and mechanical properties of the coating material, as well as the strength of the bond between coating and substrate.

Mild steel coupons, 3.2 mm thick, sprayed to coating thicknesses of 0.25 to 0.63 mm, were sectioned for hardness testing and metallographic examination. Diamond pyramid hardness (DPH) readings were taken on mounted, polished plane sections parallel to the interface, using a Vickers instrument at 2.5-kg load. Optical micrographs were made of as-polished and glyceric acid-etched transverse sections. Coating porosity was measured with an image analyzer, with the value being taken as the mean area fraction of voids at five positions on the specimen.

Bond strengths of the coatings were measured following ASTM Standard C 633-79. Coatings were sprayed onto the roughened flat end of a mild steel cylinder, 25.4 mm in diameter, that had been ground in a jig to achieve flatness. The internally threaded cylinder was then sandblasted and epoxied to a mating cylinder. The epoxy Armstrong A-2/E was

oven-cured 1 h at 93° C. Testing was performed on a tensile testing machine at 1.3 mm/min crosshead speed.

Specimens for abrasion wear testing were spray-coated mild steel plates 102 by 102 by 3.2 mm. The coatings were ground to a 60-grit finish [approximately 250 to 500 mm (AA)]. The abrasion screening wear testing was performed on a Teledyne-Taber Model 505 Abraser (fig. 8) modified to accept loads of up to 7.7 kg per wheel. Most of the testing was done at 2.9 kg per wheel. At least three specimens of each coating were run, at 1,000-cycle increments, to 10,000 or 11,000 cycles. The CS10 abrasive wheels, of rubber-bonded alumina, were refaced every 1,000 cycles.

Spray-coated bond-strength cylinders, ground to <250 nm (AA), were used for adhesive wear testing. A commercially available fatigue tester was modified to allow loading of the specimen onto a rotating 12.7-mm-wide by 47.5-mm-diam M2 tool steel wheel, hardened to R_c62, at loads of up to 40 kg. Tests were run for 1,475±25 cycles at 100 to 200 rpm, at ambient temperature in air with no lubrication. Wheels and specimens were vapor-degreased prior to testing. The wear in this screening-type test was expressed in terms of a wear volume, calculated from the specimen weight loss and the coating density. The modified apparatus is shown in figure 9.

RESULTS

The sprayed coatings displayed some physical properties different from those of the cast material of the same composition. Although the castings were intended for material characterization studies and not for wear-resistant applications, it is of interest to compare the coatings to them. Data are presented in terms of titanium diboride contents calculated from analyzed boron levels of the mechanically alloyed powders. Because the actual disposition of the boron and titanium in the sprayed coating is uncertain, as discussed below, the term "TiB₂ equivalent" is used here also.

The photomicrographs in figure 10 show that the coatings are relatively nonporous. The measured porosity, shown in figure 11, increases linearly in proportion to the TiB₂ content to a maximum of 4.4 vol pct. As porosity increases, the individual pores become interconnected, thereby creating a conduit for atmospheric corrodants to reach and attack the substrate. Interconnection has been reported to begin at just over 4 pct porosity (16); thus, these coatings may be considered protective.

The eutectic carbide phase and the proeutectic blocky TiB₂ and acicular ferrite

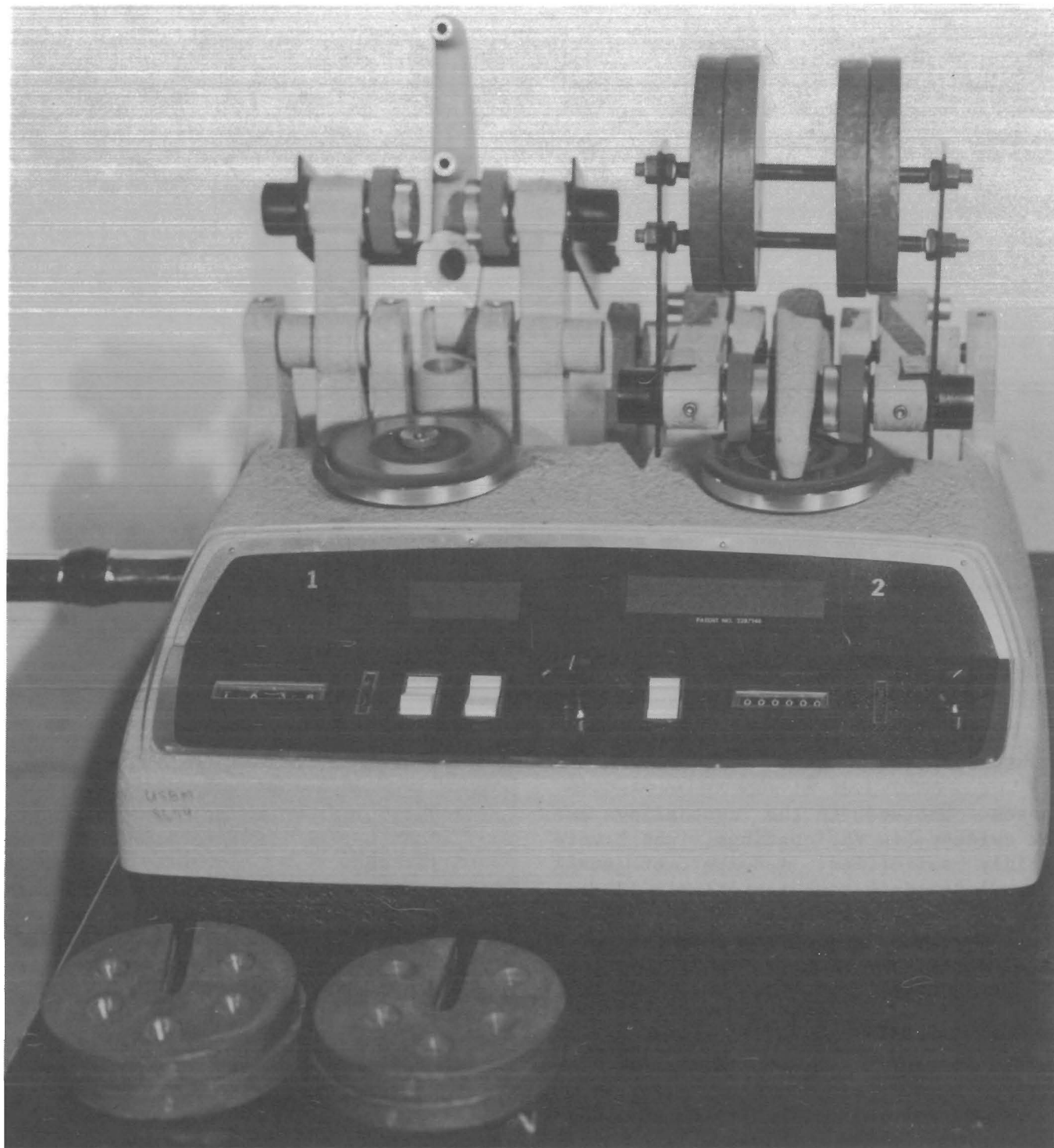


FIGURE 8. - Abrasive-wear test apparatus. A modified Taber abrasive tester showing rotating wear-test plates, rubber-bonded alumina wheels, and added weights. The vacuum pickup removes abraded particles,

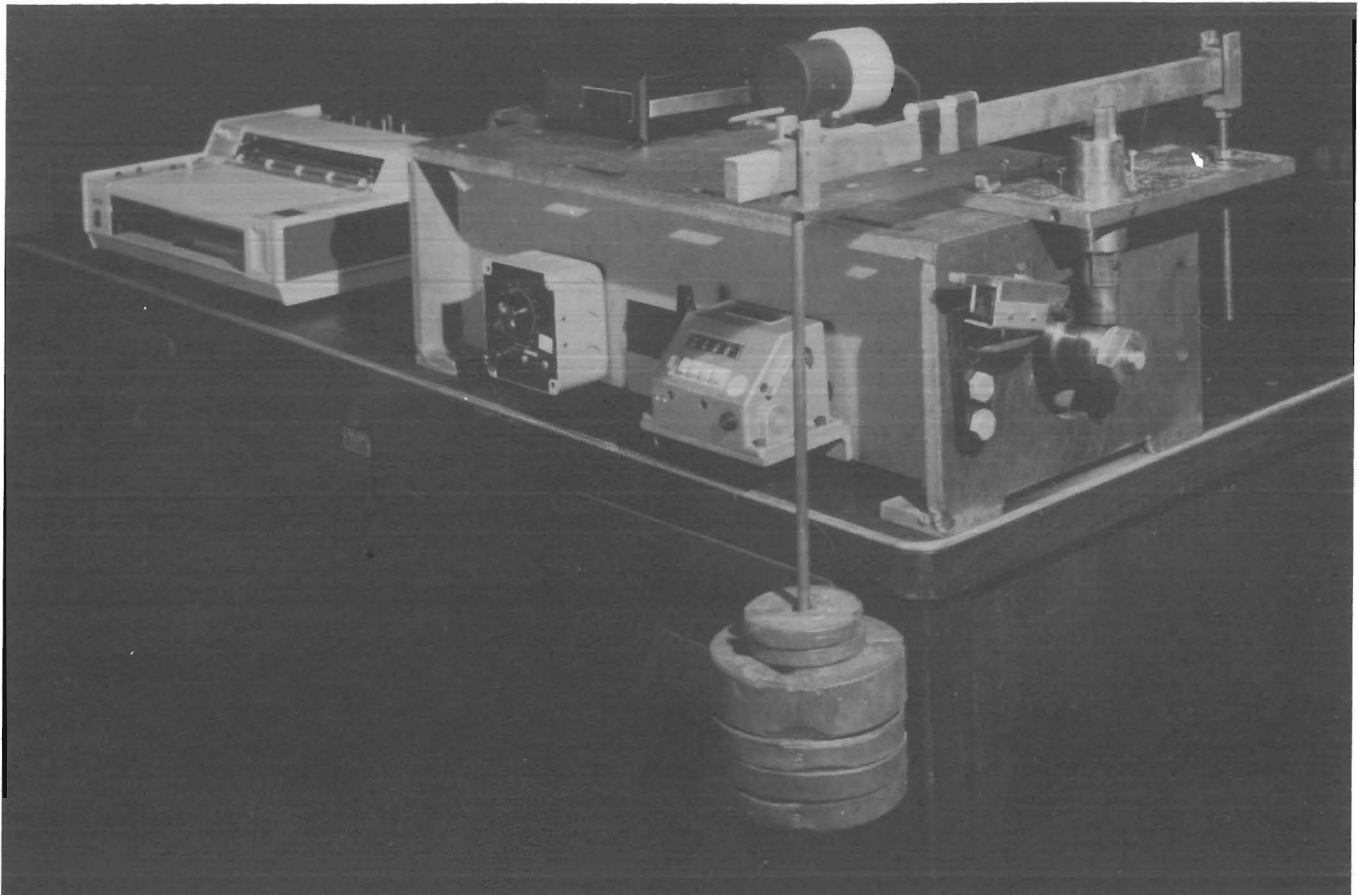


FIGURE 9. - Adhesive-wear test apparatus. In a modified fatigue tester, a loaded plasma-sprayed specimen (face down) contacts the rotating M2 tool steel wheel. A tachometer and chart recorder monitor rotation speed.

phases observed in the cast alloys are not evident in the coatings, which were rapidly solidified. A number of small ($<1\text{ }\mu\text{m}$) precipitates, tentatively identified as TiO_2 , appear in the grains. The white spots represent light reflected from asperities and shallow cavities. The stringerlike second phase, manifest also at the dark bulkier phase in figure 10A, is an Fe-Cr oxide, probably formed as an oxide skin on the molten particles during spraying. In these transverse views, the shapes of the flattened solidified droplets are outlined by the oxide stringers. The scratched area in figure 10A is part of the softer steel substrate. The total oxygen content of the coatings dropped linearly from 3.4 wt pct in MA1 to 1.8 wt pct in MA4 (oxygen content data for MA5 are not available). A mechanism explaining this behavior is discussed in the next section.

The variation in hardness of the coatings with varied TiB_2 (equivalent) content is shown in figure 12. Below 6 wt pct TiB_2 , the hardness increases nearly linearly. The reason for the dropoff above about 7.5 wt pct TiB_2 is unclear. It is noteworthy that the coatings are twice as hard as their cast counterparts in the linear region. Quenching stresses, solid-solution hardness, oxides, and very fine precipitates of carbon or boron plus carbon undoubtedly are responsible, in addition to presumed better retention of TiB_2 as fine discrete particles. In comparison, the hardness of the spray-coated Stellite 6 coating specimens averaged 470 DPH.

Coating ductilities were not measured quantitatively; qualitatively, all were brittle. Thin (1.6 mm) mild steel strips plasma-spray coated to 0.25-mm thickness could be bent only 5° to 7° before the

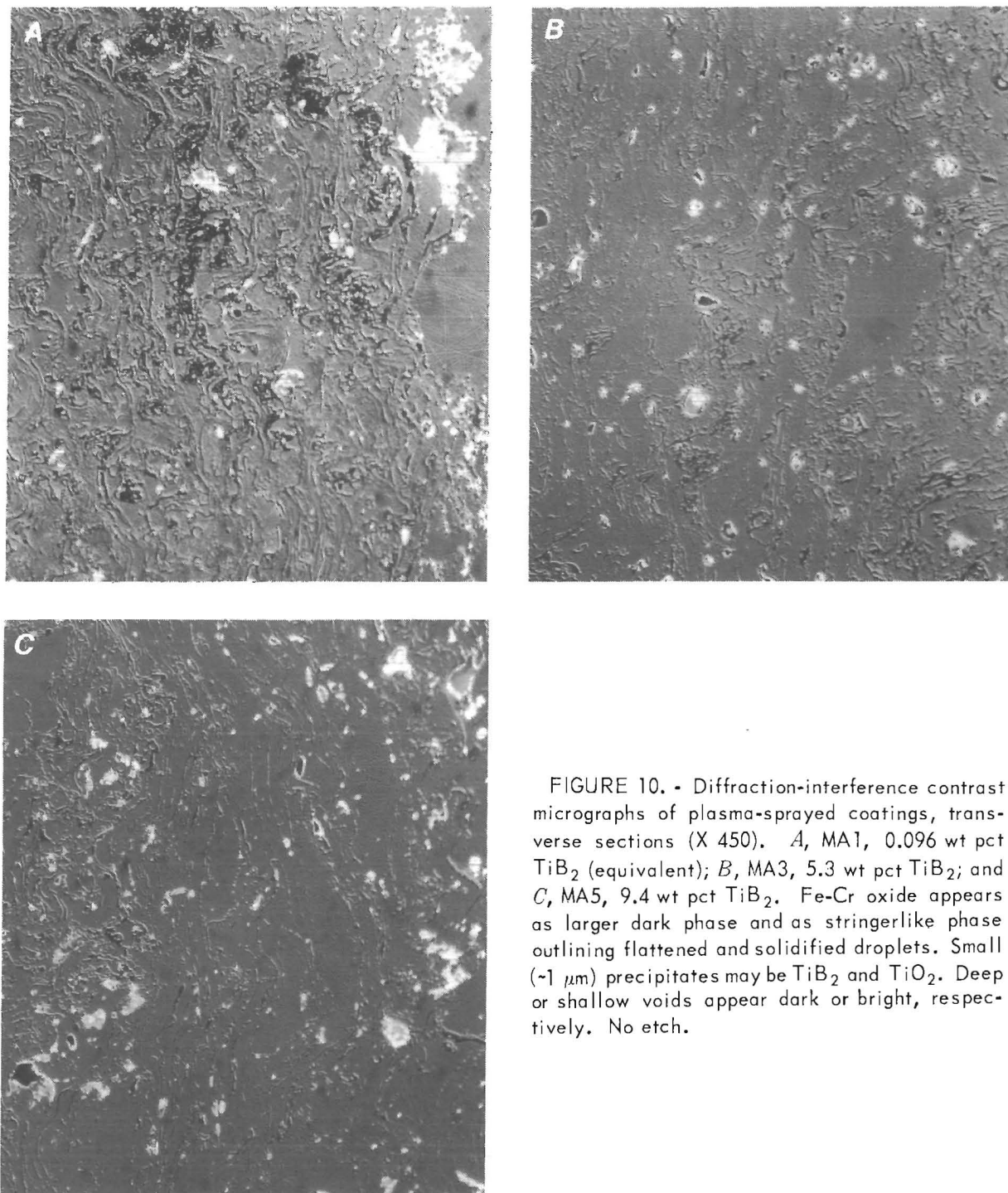


FIGURE 10. - Diffraction-interference contrast micrographs of plasma-sprayed coatings, transverse sections (X 450). *A*, MA1, 0.096 wt pct TiB_2 (equivalent); *B*, MA3, 5.3 wt pct TiB_2 ; and *C*, MA5, 9.4 wt pct TiB_2 . Fe-Cr oxide appears as larger dark phase and as stringerlike phase outlining flattened and solidified droplets. Small ($\sim 1 \mu\text{m}$) precipitates may be TiB_2 and TiO_2 . Deep or shallow voids appear dark or bright, respectively. No etch.

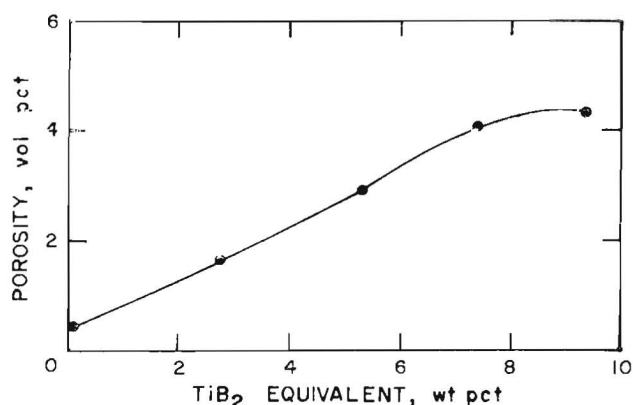


FIGURE 11. - Porosity of plasma-sprayed coatings as a function of TiB_2 (equivalent) content.

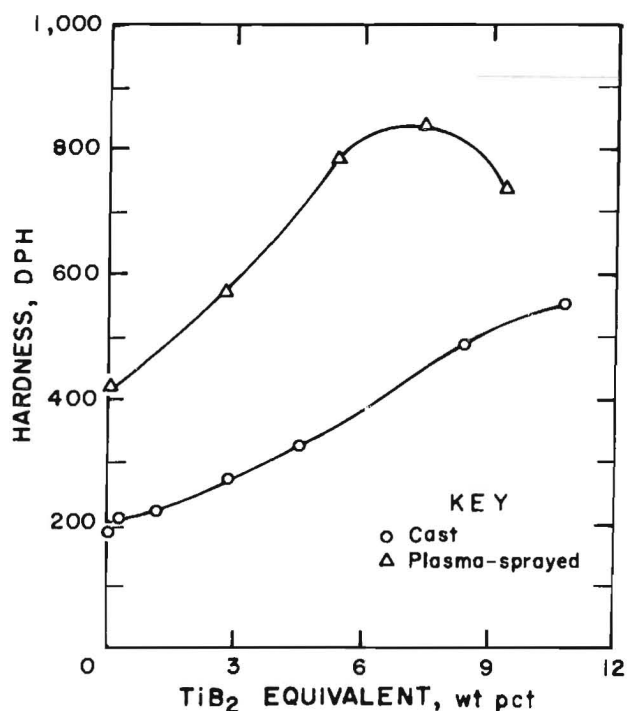


FIGURE 12. - Hardness of cast and plasma-sprayed alloys as influenced by TiB_2 (equivalent) content.

coating cracked and separated from the bend.

The bonding of the coatings to the mild steel substrates was moderately strong and relatively independent of boron content. The bond strengths in table 6 all reflect delamination of the coatings from the substrate, rather than coating fracture or epoxy failure. Within each alloy group, spraying conditions remained essentially uniform, yet bond-strength variability is quite

TABLE 6. - Bond strengths of plasma-sprayed coatings on mild steel

Coating	Bond strength, MPa	Deviation at 90 pct confidence level, MPa
MA1.....	25.8	9.4
MA2.....	34.9	7.3
MA3.....	34.6	5.6
MA4.....	34.6	9.6
MA5.....	34.9	11.9
Stellite 6	22.4	2.3

high, reaching ± 36 pct for the MA1 group. Parts of the delaminated substrate surfaces of these specimens displayed a distinct blue color, characteristic of a thin oxide film formation. Bond-pair specimens with minimal visible substrate contamination had strengths of about 35 MPa, in line with the other compositions. Substrates of these specimen pairs retained their original color.

After an initial 1,000-cycle "break-in" run, the abrasive wear of each of the coatings was linear with time over the duration of the test. Typical weight-loss patterns are seen in figure 13, which presents the wear test results for three specimens of alloy MA4 (7.4 wt pct TiB_2). Wear rates were determined by least-squares fits to the data. Mean values are plotted against TiB_2 content in figure 14. To better compare the alloys with Stellite 6, these weight losses have been converted to volume losses using the measured coating densities. The general decrease in wear rate with higher boride content is not unexpected in that the coating hardness increases with boride content.

Adhesive wear tests generated data with considerably more scatter than did the abrasive wear tests. Data for the iron-base coating-alloy compositions are compared with data for in-house plasma-sprayed Stellite 6 in table 7. Order-of-magnitude variations in the wear volume appear with specimens of the low-boride coating (MA1) and the highest boride coating (MA5). The trend is toward slightly lower wear in the material containing about 3 to 5 wt pct TiB_2 .

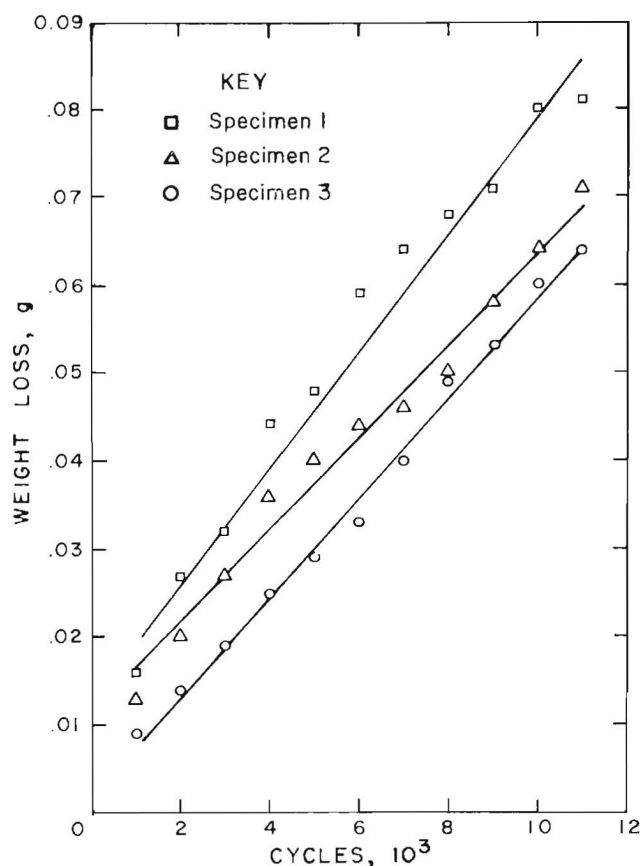


FIGURE 13. - Linear relationship between abrasive weight loss of three specimens of plasma-sprayed alloy MA4 (7.4 wt pct TiB_2) and number of cycles of abrading wheel.

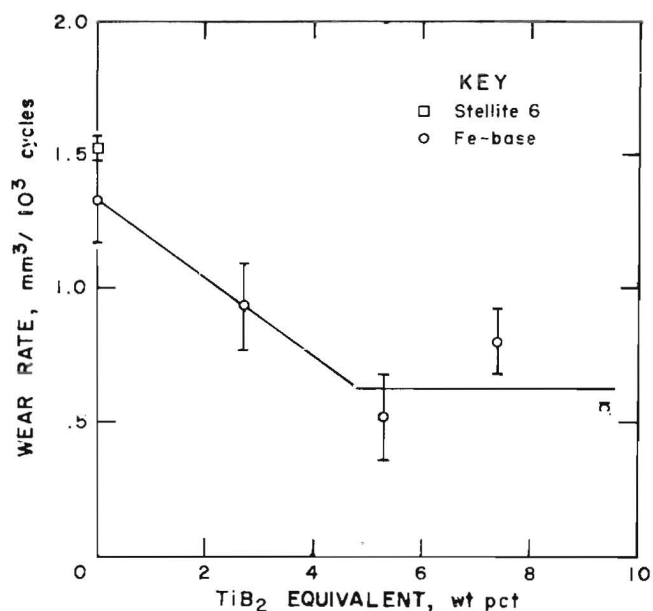


FIGURE 14. - Abrasive-wear rates of plasma-sprayed coatings as a function of TiB_2 equivalent.

A characteristic feature of the wear patterns of these coatings is a rough surface indicative of material ablation. This "bulk" removal of material is more predominant at higher boride levels. The MA5 coatings (9.4 wt pct TiB_2) fractured at the leading edge of the wear track causing gouging of the coating as the particles were dragged through by the wheel. This was not observed in the other alloys.

TABLE 7. - Adhesive wear data for plasma-sprayed coatings

Alloy	Wear volume, mm^3	Mean wear volume, mm^3	Alloy	Wear volume, mm^3	Mean wear volume, mm^3
MA1.....	2.3	3.7	MA4.....	2.4	3.7
	10.7			5.1	
	1.1			4.0	
MA2.....	.6	1.3	Stellite 6..	.4	2.2
	1.4			.3	
	2.2			3.8	
	1.1			2.6	
MA3.....	.6	1.3		3.4	3.6
	1.2			6.1	
	1.6			2.4	
	1.4			2.7	
	1.6				
	.6				

DISCUSSION

The coatings produced by plasma spraying of MA powders were sufficiently non-porous as to prevent interconnection of the substrate to the coating surface. The coatings would thus exclude corrosive fluids, thereby providing corrosion protection for the substrate, to the extent of the alloy's resistance.

The obvious differences in microstructures between the sprayed and cast material at the same nominal boride levels are attributed primarily to the much faster solidification and cooling of the sprayed coatings. The increased hardness of the sprayed coatings relative to the cast alloys also suggests a solution- or precipitation-hardening mechanism. Although the solidification and cooling rates are rapid, they are not known with any degree of certainty; hence, the extent of solid-solution quenching of the carbon is also not known. Another key question in the plasma spraying of these MA powders is to what degree the TiB_2 is retained as discrete particles, rather than dissolving and reprecipitating as finer TiB_2 or other metal boride. Very few (≤ 1 vol pct) relatively large (5 to 10 μm) TiB_2 particles were identified in the coatings, although more than 60 pct of the starting TiB_2 powder exceeded this size. Much of this fraction was, however, reduced in size by attrition grinding during milling, as seen by the lack of discrete larger particles imbedded in the powder in figure 5. Smaller 1- to 2- μm particles were seen in higher magnification photographs of these powders.

Of these smaller particles, there exists some evidence to support a small amount of dissociation. In thermal analysis of a mixture of elemental iron and titanium diboride powders at a heating rate of $10^\circ\text{C}/\text{min}$, small peaks corresponding to the Fe-B and Fe-Ti eutectics were observed, with a major peak occurring at a temperature between these two. No peak corresponding to that of elemental iron was seen. The conclusion is that the boride dissociated to a small

extent below $1,160^\circ\text{C}$ (the Fe-B eutectic), then caused a eutectic-type melting of the mixture at $1,285^\circ\text{C}$. Research in progress is addressing the disposition of sized TiB_2 in similar alloy matrices throughout the mechanical alloying and plasma spraying operations.

A portion of the boron was lost completely from the alloy during spraying, as determined by chemical analysis of the coatings. This loss can be accounted for by a mechanism by which the boron "intercepts" some of the oxygen picked up by the molten particles in the plasma flame and removes it. Boron will oxidize preferentially to titanium or chromium. With the vaporization temperature of B_2O_3 being $2,017^\circ\text{C}$, it is conceivable that some of the oxide would heat to this temperature and escape from the surface of the liquid metal droplet. The oxygen removed during spraying of a given coating was estimated from the differences between the nominal and analyzed boron contents in the coating, using the relationship, $2\text{B} + 3/2\text{O}_2 = \text{B}_2\text{O}_3$, and substituting the measured boron losses for B. Assuming the oxygen content in MA1 to be the "nominal" oxygen level attained in any of the alloy coatings in the absence of boron, the reduction in oxygen can be ascribed to that removed by the boron as B_2O_3 vapor. The calculated and measured values, plotted in figure 15, agree quite well. This argument can account for about one-third of the nominal starting boron contained in the TiB_2 .

Compared with in-house sprayed Stellite 6, the TiB_2 alloy system has performed well; bond strength as well as abrasive and adhesive wear resistance are all superior. In absolute value, however, the bond strength of the coatings may be open to some question; at 35 MPa, the bonding is marginal. This may be due to a substrate roughness (upon which the mechanical keying of the coating depends) of only 5 μm (AA), the maximum achievable with the particular grit-blast system used. Improvements in bond strengths of

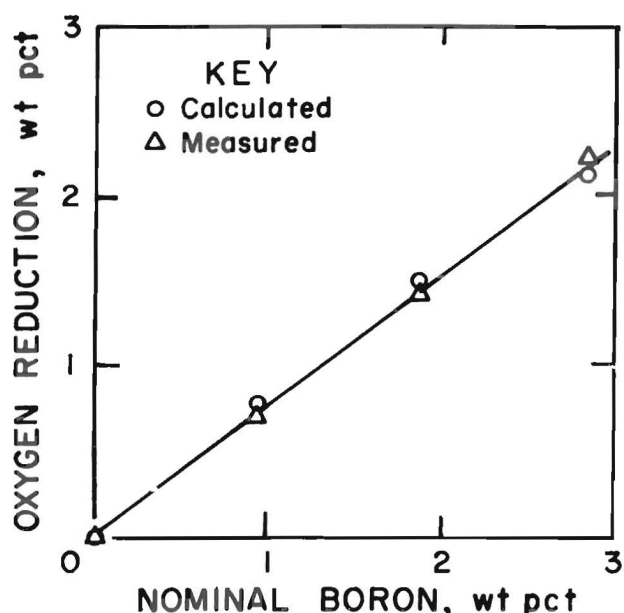


FIGURE 15. - Relation between decrease in oxygen content of plasma-sprayed powders and nominal boron content. Calculated values determined using the relationship $2B + 3/2O_2 = B_2O_3$ and the measured boron loss values.

40 to 60 pct with surface roughness increasing from <5 to 8.9 or 10.7 μm (AA) have been reported (17). Inclusion of TiB_2 did improve the bond strength by 9 MPa over that of the alloy without added boride. It has not been determined

whether this was due to direct effects such as oxide fluxing by the boron or boron oxide, or to indirect effects related to powder morphology. Improved bonding of these alloys is under current investigation.

It must be emphasized that the two wear tests used were for comparative screening; as such, the magnitude of the numerical values of the results may be of minimal consequence. The two wear screening tests indicated a slight advantage to the intermediate boride alloy containing 5.3 wt pct TiB_2 (MA3), with the best combination of abrasive and adhesive wear. Among the abrasive wear specimens, the only observed qualitative differences were fewer and shorter scratches in the wear track as boride content increased. Matrix hardness is the apparent controlling factor here rather than the size or volume fraction of hard particles. Although results for the 7.4 wt pct TiB_2 alloy (MA4) were inconclusive, the trend toward greater wear resistance with increased boride is evident. Additional wear testing, following ASTM standards, is planned for the in-house prepared Stellite material and the optimum experimental coating composition, MA3, containing 5.3 wt pct TiB_2 .

SUMMARY AND CONCLUSIONS

An alloy system with Fe, 19 wt pct Cr, 9 wt pct Ni, carbide formers, and TiB_2 added to 12 wt pct nominal has been investigated as a potential replacement for some conventional wear-resistant, cobalt-based hardfacing alloys. A pseudobinary phase diagram was constructed showing a eutectic at 1,210° C and 5.5 wt pct TiB_2 . The hypoeutectic alloys solidified into a dendritic structure, while above, proeutectic blocky TiB_2 and acicular ferrite phases appeared.

Metal powders covering the same compositional range were prepared by mechanical alloying for subsequent plasma spraying onto mild steel coupons. The coatings produced were dense, with a network of oxides and a distribution of fine precipitates, leading to hardnesses

about double those of the castings at the same compositions. The coating-to-substrate bond strength, abrasive wear, and metal-to-metal (adhesive) wear were superior to those of plasma-sprayed Stellite 6. The optimum TiB_2 level was at about 5 wt pct.

In this initial investigation of the carbide-strengthened, boride-bearing, iron-base alloy system, the potential to compete with Stellite for some uses has been demonstrated. Additional properties, including hot hardness, corrosion and oxidation resistance, and thermal stability need to be evaluated. Improved bonding is desirable. Research in these areas, as well as weld deposition of thicker coatings of these alloys, is underway or planned.

REFERENCES

1. Mathews, S. J. Potential for Hard-Facing Application Technology To Conserve Critical Metals. Vanderbilt Workshop on Conservation and Substitutes Technology for Critical Materials, v. II, June 1981, pp. P25-1 to P25-9.
2. American Welding Society. Specification for Surfacing Electrodes and Welding Rods. A 5.13-80, 1980, 22 pp.
3. Schumacher, W. J. A Stainless Steel Alternative to Cobalt Wear Alloys. Chem. Eng., v. 88, No. 19, Sept. 21, 1981, pp. 149-152.
4. Cabot Corp., Wear Technology Division (Kokomo, IN). Cobalt Alloy Used in Critical Spots of Continuous Pulp Digester. Stellite Digest, v. 27, No. 1, 1976, 4 pp.
5. Wall Colmonoy Corp., Detroit, MI. Colmonoy Technical Data Sheet T-29. 1977, 2 pp.
6. Collopy, W. F. Powders Add Flexibility to Hardfacing, Cut Costs. Met. Prog., v. 121, No. 6, May 1982, pp. 47-49.
7. Cabot Corp., Wear Technology Division (Kokomo, IN). Stellite Hard-Facing Products. 1975, 23 pp.
8. Hickl, A. J. Nickel-Base Alloys as Alternatives to Cobalt-Base Alloys for P/M Wear and Environmental Resistant Components. Mod. Dev. in P/M, v. 14, 1981, pp. 455-466.
9. Patel, M. New Cobalt Reduced Hardfacing Alloys. Paper in Wear and Fracture Prevention (Proc. Conf. Peoria, IL, May 21-22, 1980). Am. Soc. Metals, Metals Park, OH, 1980, pp. 121-132.
10. Matlock, W. M. Development of an Iron Base Hardfacing for Internal Combustion Engine Valves. Paper in Wear and Fracture Prevention (Proc. Conf. Peoria, IL, May 21-22, 1980). Am. Soc. Metals, Metals Park, OH, pp. 277-288.
11. Whelan, E. P. Hardness and Abrasive-Wear Resistance of Ni-Cr-Mo-C Hardfacing Alloys. J. Met., v. 31, No. 1, 1979, pp. 15-19.
12. Pickering, F. B. Physical Metallurgy of Stainless Steel Developments. Int. Metals Rev., v. 21, Dec. 1976, pp. 226-268.
13. Engineering Alloys Digest, Inc., Upper Montclair, NJ. Alloy Digest, SS-319, Nov. 1975, 2 pp.
14. Shurin, A. K., and N. A. Raznmova. Quasiternary System Fe-TiC-TiB₂. Sov. PM Metall. Ceram., v. 18, No. 12, 1979, pp. 903-905.
15. Benjamin, J. S. Dispersion Strengthened Superalloys by Mechanical Alloying. Met. Trans., v. 1, No. 10, 1970, pp. 2943-2951.
16. Hausner, H., and M. K. Mal. Handbook of Powder Metallurgy. Chem. Publ. Co., 2d ed., 1982, p. 507.
17. Roseberry, T. J., and F. W. Boulger. A Plasma Flame Spray Handbook. Batelle Mem. Inst., Columbus, OH. Rep. MT-043, Mar. 1977, 161 pp.